Thermal Conductivity and Morphology of Silver-Filled Multiwalled Carbon Nanotubes/Polyimide Nanocomposite Films

I-Hsiang Tseng, Hsin-Chuan Lin, Mei-Hui Tsai, Dong-Sen Chen

Department of Chemical and Materials Engineering, National Chin-Yi University of Technology, Taichung 41170, Taiwan

Received 27 April 2011; accepted 23 January 2012
DOI 10.1002/app.36905
Published online in Wiley Online Library (wileyonlinelibrary.com).

ABSTRACT: A facile methodology has been developed to synthesize silver-filled multiwalled carbon nanotubes (S-MWNTs)-polyimide (PI) nanocomposites with high thermal conductivity for applications in flexible printed circuits or buried film capacitors, requiring efficient heat dissipation. MWNTs functioned as modules to facilitate the distribution of Ag particles within PI matrix. The intercalation of Ag within MWNTs was performed using capillary action upon mixing $AgNO_3$ solution with PI precursor and followed by calcinations to reduce the ionic silver to Ag. The existence of Ag in the PI nanocomposites was observed from transmission electron microscope images and verified with the energy-dispersive X-ray spectrometer. Homogeneous dispersion of SMWNTs in PI matrix and strong interaction between S-MWNTs and PI were also suggested by SEM cross-section images. The thermal conductivity of S-MWNT/PI nanocomposite was a function of the content of S-MWNTs in PI matrix. The PI nanocomposite containing 1.5 wt % of S-MWNTs (S-MWNT/PI-1.5) exhibited the highest thermal conductivity, 0.37 W/mK. A decrease in thermal conductivity was observed while the surface roughness of the nanocomposite was higher than 1 μm owing to the high content of S-MWNT in PI. In addition, the modified MWNTs improved flexibility of the PI matrix. © 2012 Wiley Periodicals, Inc. J Appl Polym Sci 000: 000–000, 2012

Key words: polyimide; multiwalled carbon nanotube; silver; thermal conductivity; capillary action; nanocomposite

INTRODUCTION

Carbon nanotubes (CNTs) have been widely utilized as fillers in polymeric nanocomposites to improve the composite properties owing to the excellent mechanical strength and superior thermal and electrical conductivities of CNTs.[1–8] The intercalation of metals within CNTs using capillary action or decoration of metals on the surface of CNTs has been commonly applied to modify CNTs with integrated properties.[5,9–13] For example, Ma and Lee et al.[5,12] prepared silver-decorated CNTs to increase the electrical conductivity and optical transmittance of CNTs. Polyimides (PIs) with good chemical resistance, superior thermal stability, and high mechanical strength are widely applied in electronic and aerospace industry.[14–17] With the addition of single-walled or multiwalled carbon nanotubes (SWNTs or MWNTs) in the PI matrix, the nanocomposites will have improved thermal conductivity, mechanical strength, electrical conductivity, and dielectric constant for advanced applications.[4,6–8,15–26] Recently, Zhang et al.[8] reported an enhanced thermal conductivity of PI nanocomposite to 0.4 W/mK by incorporation of 5 wt % AlO(OH)-coated MWNTs in PI matrix compared to 0.17 W/mK for pure PI.

In this study, modification of MWNTs was successfully performed by filling with Ag from $AgNO_3$ solution, which was able to wet the surface of MWNTs owing to its low surface tension.[13] The thermal conductivity of PI nanocomposites was improved significantly to the literature reported value,[8] 0.4 W/mK, only with the addition of 1.5 wt % of S-MWNTs in PI matrix. Meanwhile, the resulting nanocomposites retain good thermal stability and film flexibility, suggesting their potential applications in electromagnetic shielding materials, capacitors, field emission materials, and aerospace materials.

EXPERIMENTAL

Materials

The MWNTs (purity, >97%) with the diameter of 10–40 nm and the length of 5–15 μm were commercial products from Advanced Nanopower Inc.

Correspondence to: M.-H. Tsai (tsaimh@ncut.edu.tw).
Contract grant sponsor: The Ministry of Economic Affairs, Taiwan; contract grant number: 99-EC-17-A-07-S1-120.

(Taipei, Taiwan). Pyromellitic dianhydride (PMDA, 99.5%, Chiskev, Leawood, KS) was purified by recrystallization with acetic anhydride (99.8%, Tedia) and then dried in a vacuum oven at 125°C over night. 4,4′-Diaminodiphenylether (ODA, 98%, Lancaster) was dried in a vacuum oven at 120°C for 3 h prior to use. *N*,*N*-dimethylformamide (DMF, Tedia) was dehydrated with molecular sieves (4 Å). Silver nitrate (S, 99.8%, Showa) was used as received.

Synthesis of S-MWNTs

As received, MWNT was purified by HNO_3 treatment and followed by heating at 673 K under air for 30 min and nitrogen for 3 h. After cooling to room temperature, the acid-treated nanotubes (A-MWNTs) were ultrasonicated in a beaker containing over-saturated $AgNO_3$ solution for 2 h. After filtration and washing with distilled water, the modified nanotubes were dried at room temperature for 48 h and followed by calcination at a heating rate of 5°C/min to 473 K (or 573 or 673 K) for 1 h under Ar to obtain S-MWNTs.

Synthesis of S-MWNTs–PI nanocomposites

The procedure to prepare the S-MWNTs–PI nanocomposite films is shown in Scheme 1. First, the S-MWNTs were dissolved in DMF in a three-necked flask in an ultrasonic bath at room temperature for at least 30 min. The ODA monomer was then added into the above solution under nitrogen at room temperature for 2 h. Subsequently, the PMDA monomer was introduced into the solution in five portions. After PMDA was completely dissolved in the solution, the mixture was further stirred for 3 h to obtain the precursor S-MWNT–polyamic acid. This precursor was coated on a glass substrate and followed by the thermal imidization process in an air-forced oven, which was isothermal for 1 h at each of the following temperature: 60, 100, 150, 200, and 300°C. The final thickness of obtained S-MWNT-PI nanocomposite films was in the range of 30–50 μm. In this article, the PI nanocomposites containing S-MWNTs were denoted by S-MWNT-PI-*x*, where *x* (0.3–10) implied the weight percentage of S-MWNT within composites. Reference samples denoted A-MWNT-PI-3 and *x*-MWNT-PI-3 were prepared by adding 3 wt % of A-MWNT or untreated MWNT (*x*-MWNT) in composites.

Measurements

The morphology of samples was analyzed by a high-resolution transmission electron microscope (JEOL JEM-2010) with the energy-dispersive X-ray spectrometer (EDS) as well as a field emission scanning electron microscope (JEOL JSM-6330F). For TEM observation, nanocomposite films were embedded into epoxy capsules and then cured at 70°C for 24 h in a vacuum oven. The sample-imbedded epoxy was then microtomed into 90-nm thick slices in the direction normal to the plane of the films with Leica Ultracut Uct. The morphology of S-MWNT powders or the fractured surfaces of S-MWNT/PI nanocomposite films was inspected by SEM. The fracture surface was obtained by breaking the cryogenic films by liquid N_2. The X-ray diffraction (XRD) analysis was carried out with the MAC Science MXP18 for powders or with the Rigaku RU-H3R for films. The dynamic mechanical analysis (DMA, TA Instruments DMA-2980) was performed from 60 to 400°C, at a heating rate of 3°C/min and at a frequency of 1 Hz. Thermogravimetric analysis (TGA, TA Instruments TGA-Q500) was performed from 60 to 900°C at a heating rate of 20°C/min under nitrogen. The thermal conductivity of the nanocomposite was measured by a hot disk sensor (TechMax H5DR). The experimental value was the averages of three measurements performed. The surface morphology and roughness of nanocomposite films were also investigated by an atomic force microscope (AFM, Digital Instrument NS4/D3100CL) under a contact mode.

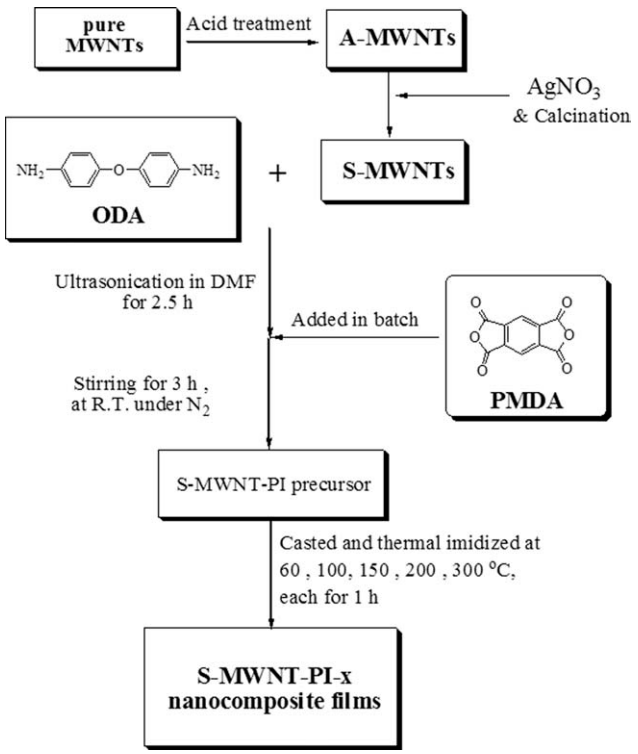

Scheme 1 Schematics of preparing S-MWNT-PI-*x* nanocomposite films.

RESULTS AND DISCUSSION

The SEM images of the fractured surface of S-MWNT-PI-10 nanocomposite are shown in

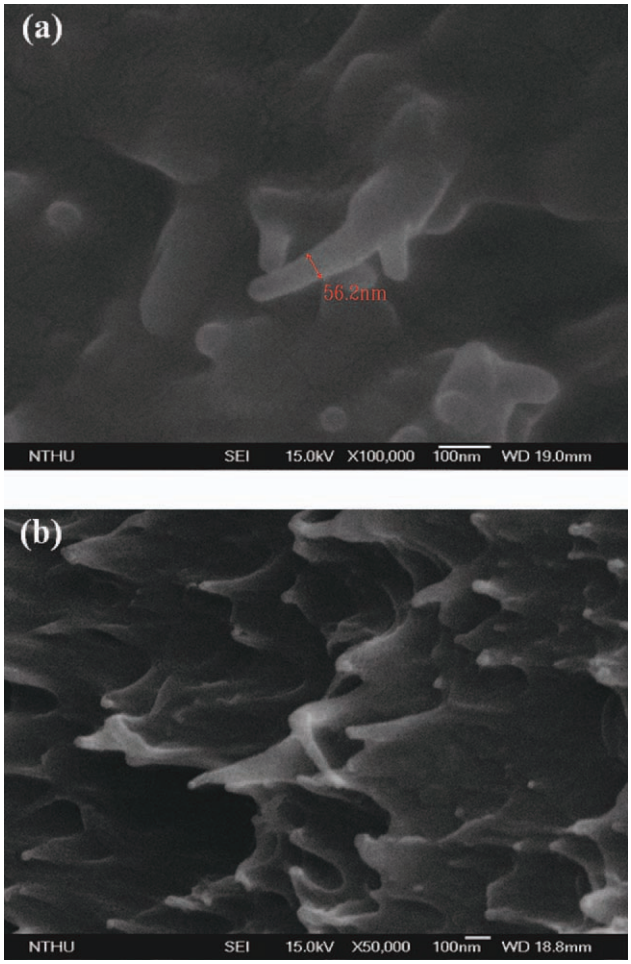

Figure 1 SEM images of S-MWNT-PI-10 hybrid film. Magnification: (a) 100 K; (b) 50 K. [Color figure can be viewed in the online issue, which is available at wileyonlinelibrary.com.]

Figure 1. The diameter of S-MWNTs in this PI nanocomposite shown in Figure 1(a) was around 56 nm, which was larger than that of S-MWNTs ranging from 20 to 30 nm, indicating the thick coating of PI on S-MWNTs and also the strong adhesion of PI to S-MWNTs. No gap between S-MWNT and PI matrix as well as no aggregates of S-MWNTs were observed in the cross-section of nanocomposites shown in Figure 1(b). Those phenomena suggested a strong bonding between S-MWNTs and PI matrix together with a homogeneous dispersion of S-MWNTs throughout the PI matrix.[6,26] The homogeneous dispersion of S-MWNTs and the tight interaction between S-MWNTs and PI at the interface lead to a higher thermal conductivity for the obtained hybrid films.

In this study, the optimum calcination temperature to efficiently reduce silver ions to silver was 473 K after comparing the filling conditions revealed from TEM images of S-MWNTs and the XRD spectra of various S-MWNT-PI nanocomposites. Figure 2(a) shows the TEM image of S-MWNTs calcinated at 473 K. Most of the silver particles deposited inside the S-MWNTs (indicated by arrows with asterisk) or on the open ends of nanotubes (indicated by arrows). The longest silver-filling length of nanotubes was around 100 nm, which was compatible to the reported metal-filling levels.[27,28] In addition, large silver particles formed and attached to the surface of MWNTs rather than inside the tubes when the heating temperature was higher than 473 K. The EDS results shown in Figure 2(b) confirmed the S-MWNT sample calcinated at 473 K containing 6.52 wt % of silver, 7.02 wt % of carbon, and 86.46 wt % of copper. The high composition of copper was owing to the usage of copper grid for TEM.

The XRD patterns of the S-MWNTs powders and S-MWNT-PI-x nanocomposite films are shown in Figure 3. The main diffraction peaks at 38 and 44° were corresponding to the 111 and 200 crystalline planes, respectively, of the cubic structure of silver.[5,9] For nanocomposite films with the content

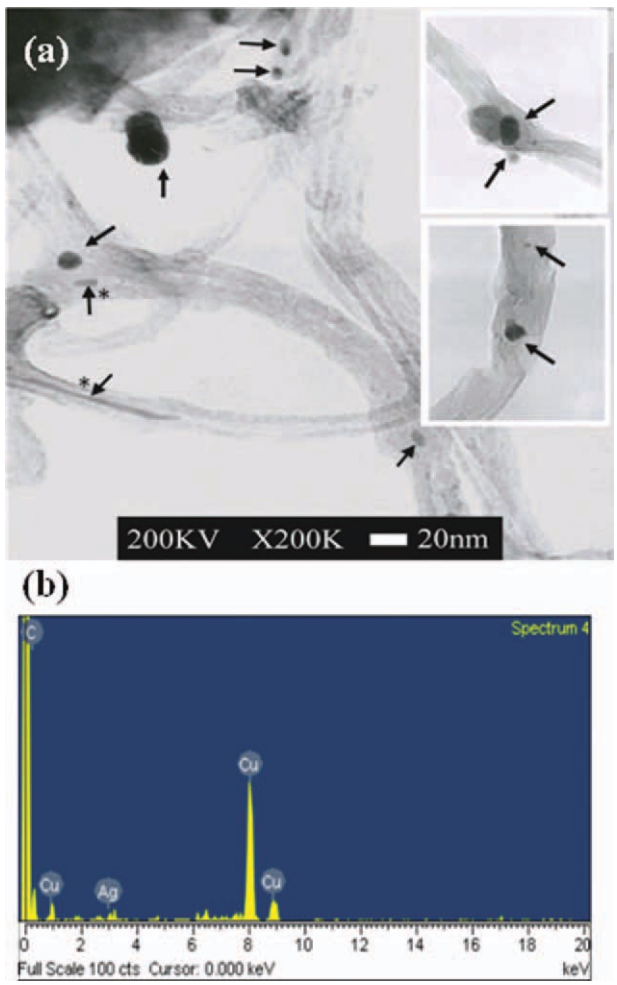

Figure 2 (a) TEM images of S-MWNTs; (b) EDS spectrum of S-MWNTs. [Color figure can be viewed in the online issue, which is available at wileyonlinelibrary.com.]

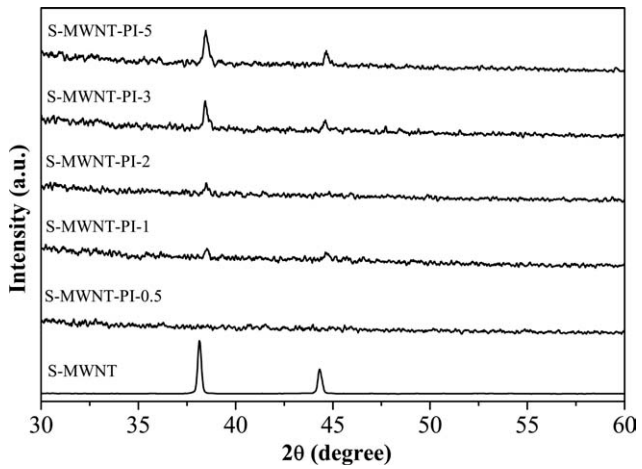

Figure 3 XRD patterns of S-MWNTs and S-MWNT-PI-*x* nanocomposite films.

of S-MWNTs <0.5 wt %, no diffraction peaks corresponding to silver can be observed. The intensity of the characteristic silver peaks increased proportionally with the content of S-MWNTs that those diffraction peaks was visible for nanocomposites S-MWNT-PI-1 to −5. The results again confirmed the successful reduction of silver precursor to silver particles during the synthesis process.

Two types of reference PI nanocomposites containing unmodified MWNTs (*x*-MWNT-PI) or only A-MWNT was prepared to investigate the effect of modification of MWNTs on the resultant properties of nanocomposite films. Figure 4 shows the tan δ as a function of temperature for the *x*-MWNT-PI-3, A-MWNT-PI-3, and S-MWNT-PI-3 nanocomposites containing same amount (3 wt %) of various MWNTs. The peak of tan δ curve was assigned as the glass transition temperature (T_g) of each hybrid

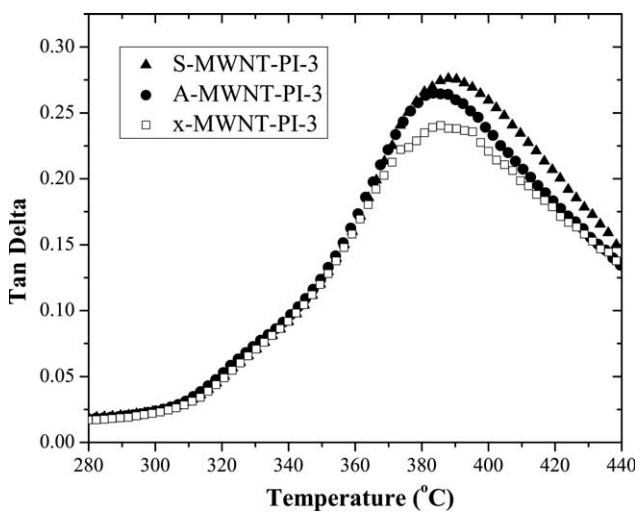

Figure 4 The tan δ curves of PI nanocomposites containing 3 wt % of unmodified (*x*−), acid-treated (*A*−), and silver-filled (*S*−) MWNTs as a function of temperature.

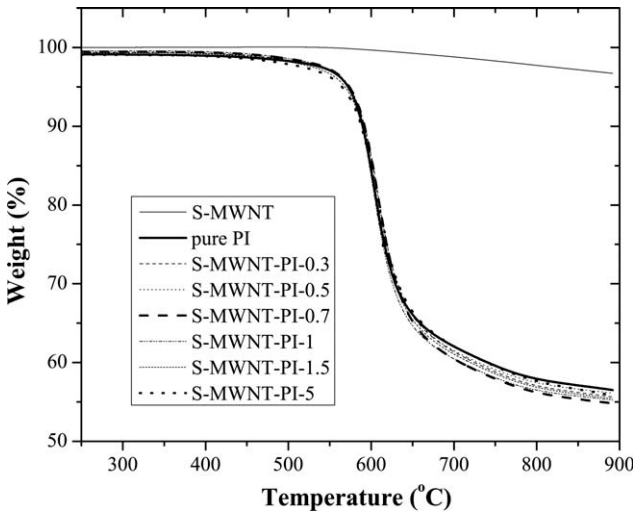

Figure 5 The TGA profile of the pure PI and S-MWNT-PI-*x* nanocomposite films.

film. The T_gs of *x*-MWNT-PI-3, A-MWNT-PI-3, and S-MWNT-PI-3 were 383, 382, and 384°C, respectively. The change in *T*g for the hybrid films containing 3 wt % of three types of MWNTs was negligible. On the other hand, the intensity of the tan δ curves indicated the damping intensity and the stiffness of hybrids. The damping intensity increased slightly when the hybrid films containing A- or S-MWNTs which have smaller length and length/width ratio than nonmodified ones. Consequently, the modified MWNTs induced the softness in hybrid films.

The TGA profiles of pure PI, S-MWNTs, and S-MWNT-PI-*x* nanocomposite films are shown in Figure 5. For pure S-MWNTs, no significant weight loss can be detected in the temperature range up to 550°C. It has been noticed that the addition of MWNTs changes the thermal stability of nanocomposites owing to the metallic residue.[25] In this study, the decomposition temperature (T_d) at 5% weight loss of pure PI was 572°C, which was lower than that of films with 0.3–0.7 wt % of S-MWNT, all around 575°C. In contrast, when the content of S-MWNTs in PI was more than 1 wt %, T_d was slightly decreased to 568°C. The char yield of all nanocomposites was smaller than that of pure PI, indicating the increase in softness of nanocomposites with the presence of S-MWNTs.

Figure 6 shows the thermal conductivity as a function of the content of various MWNTs in S-MWNT-PI hybrid films as well as three reference samples, pure PI, *x*-MWNT-PI-3, and A-MWNT-PI-3. The thermal conductivity of pure PI was about 0.2 W/mK. Adding 3 wt % unmodified MWNT in PI increased the thermal conductivity to 0.27 W/mK. A significant decrease in thermal conductivity of the hybrid film containing 3 wt % acid-treatment MWNTs (A-MWNT-PI-3) was observed. The cutoff

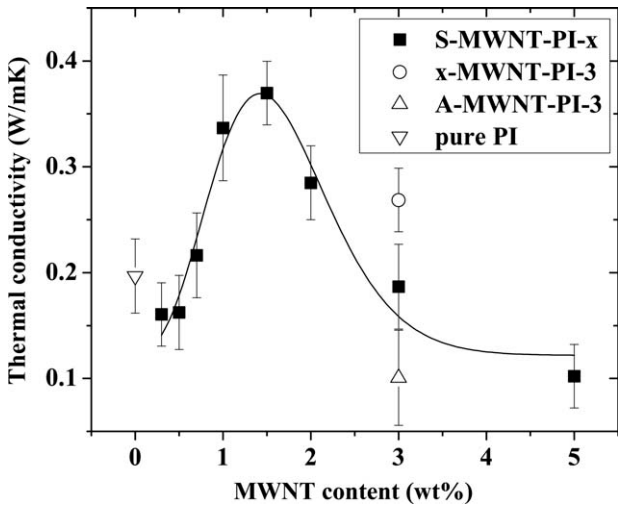

Figure 6 Effect of MWNTs content on thermal conductivity of various MWNT-PI nanocomposites.

of MWNTs during acid treatment leads to a lower aspect ratio of A-MWNTs and consequently reduces their thermal conductivity. After filling with silver in MWNTs, the electron transfer ability was restored that the thermal conductivity of hybrid films was largely improved simultaneously. When the S-MWNT content was <1.5 wt %, the thermal conductivity of hybrid films increased with the content of S-MWNT. The S-MWNT-PI-1.5 exhibited the highest thermal conductivity, close to the highest literature value of 0.4 W/mK.[8] However, the more S-MWNT addition increased the surface roughness as confirmed with the AFM images shown in Figure 7 that the thermal conductivity of S-MWNT-PI-5 was lower than pure PI. Similar trend was observed from the previous results,[17] where the decrease in mechanical strength was observed when the composition of S-MWNT in PI was higher than 1.5 wt %. The mean roughness (R_a) of hybrids containing 1, 1.5, and 3 wt % of S-MWNTs was 300–400 nm, 600–700 nm, and 1 μm, respectively. The surface roughness of PI nanocomposite higher than 1 μm was believed to trap significant amount of air at the interface of the probe and sample during measurements by hot disk sensor. In addition, too many S-MWNTs in PI matrix might increase the free volume of PI nanocomposite and thus the thermal resistance was increased.

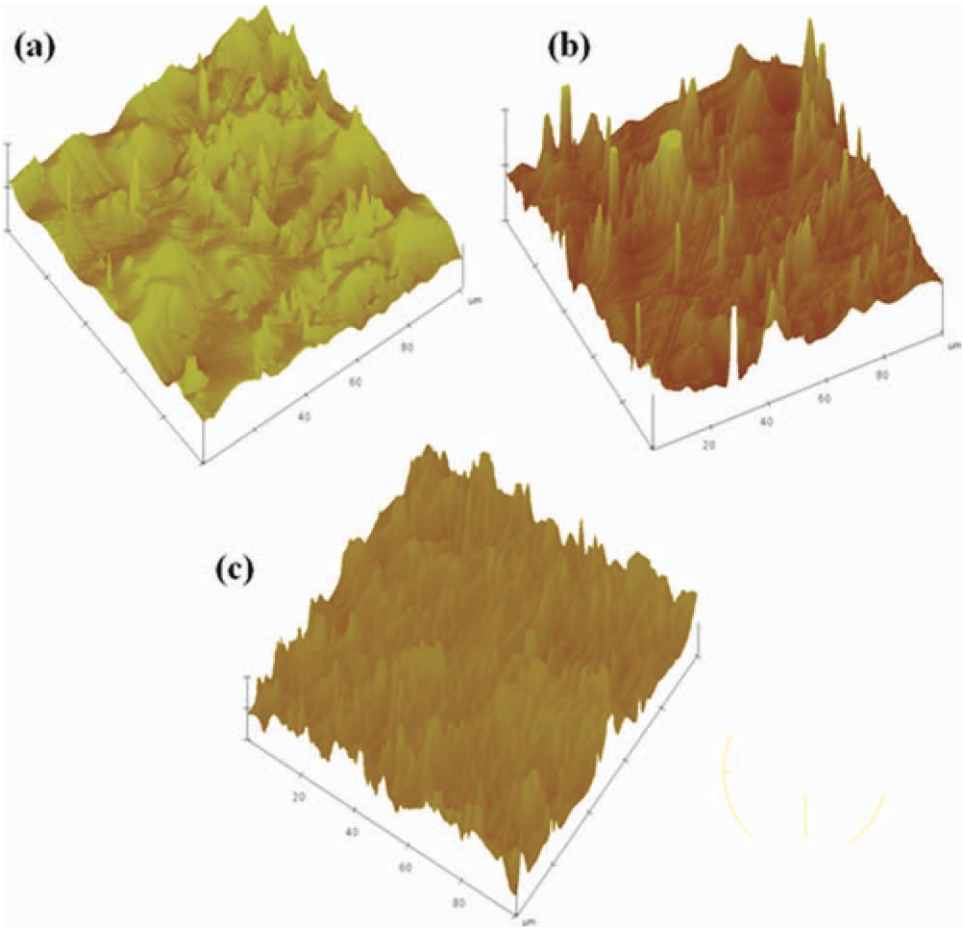

Figure 7 AFM images of hybrid films (a) S-MWNT-PI-1; (b) S-MWNT-PI-1.5; (c) S-MWNT-PI-3. [Color figure can be viewed in the online issue, which is available at wileyonlinelibrary.com.]

CONCLUSIONS

MWNTs functioned as nanomodules to disperse silver within PI matrix by capillary action and followed by calcination in Ar. MWNTs after acid treatment and silver filling were homogeneously dispersed in PI matrix and strong bonded to PI matrix as confirmed with SEM and TEM images. The presence of Ag in MWNTs was evidenced by EDS and XRD results. The Tg of S-MWNT-PI-x nanocomposite films was at least 400°C and the T_d was around 550°C, indicating that the addition of S-MWNT does not decrease the thermal stability of PI hybrid films. Notably, the thermal conductivity of hybrid film was proportional to the content of S-MWNT <2 wt %. The hybrid film with only 1.5 wt % S-MWNTs in PI matrix (S-MWNT-PI-1.5) showed the highest thermal conductivity, 0.37 W/mK, which was close to the literature-reported value. The PI nanocomposites with excellent thermal conductivity, sufficient thermal stability, and good film flexibility are potential materials for the applications in flexible printed circuits or buried film capacitors requiring efficient heat dissipation.

References

1. Iijima, S. H.; Nature 1991, 354, 56.
2. Sivakumar, R.; Guo, S.; Nishimura T.; Kagawa, Y. Scr Mater 2007, 56, 265.
3. Peng H.; Jain M.; Peterson D. E.; Zhu, Y.; Jia, Q. Small 2008, 11, 1964.
4. So, H. H.; Cho, J. W.; Sahoo, N. G. Eur Polym Sci 43, 3750.
5. Ma, P. C.; Tang, B. Z.; Kim, J. K. Carbon 2008, 46, 1497.
6. Yuan, W.; Che, J; Chan-Park, M. B. Chem Mater 2011, 23, 4149.
7. Min, C.; Shen, X.; Shi, Z.; Chen, L.; Xu, Z. Polym Plast Technol 2010, 49, 1172.
8. Zhang, Y.; Xiao, S; Wang, Q.; Liu, S.; Qiao, Z.; Chi Z.; Xu, J. Economy J. J Mater Chem 2011, 21, 14563.
9. Wu, H. P.; Wu, X. J.; Ge, M. Y.; Zhang, G. Q.; Wang, Y. W.; Jiang, J. Comp Sci Technol 2007, 67, 1182.
10. Guo, D.; Li, H. L. Carbon 2005, 43, 1259.
11. Dujardin, E.; Ebbesen, T. W.; Hiura H.; Tanigaki K. Science 1994, 265, 1850.
12. Lee, S. H.; Teng, C. C.; Ma, C. C. M.; Wang, I. J Colloid Interface Sci 2011, 364, 1.
13. Ebbesen, T.W. J Phys Chem Solids 1996, 57, 951.
14. Xiao, Y. C.; Dai, Y.; Chung, T. S.; Guiver, M. D. Macromolecules 2005, 38, 10042.
15. Tang, Q. Y.; Chan, Y. C.; Wong, N. B.; Cheung, R. Polym Int 2010, 59, 1240.
16. Park, C.; Ounaies Z.; Watson, K. A.; Crooks, R. E.; Smith, J., Jr.; Lowther S. E.; Connell, J. W.; Siochi, E. J.; Harrison, J. S.; St. Clair, T. L. Chem Phys Lett 2002, 364, 303.
17. Tsai, M. H.; Chen, D. S.; Chiang, P. C.; Lin H. C.; Jehng, J. M. J Nanosci Nanotechnol 2008, 8, 2671.
18. Thuau, D.; Koutsos, V.; Cheung, R. J Vac Sci Technol B 2009, 27, 3139.
19. Pérez, R. J Appl Polym Sci 2009, 113, 2264.
20. Srivastava, R.; Banerjee, S.; Jehnichen, D.; Voit B.; Böhme, F. Macromol Mater Eng 2009, 294, 96.
21. Singh, B. P.; Singh, D.; Mathur R. B.; Dhami, T. L. Nanoscale Res Lett 2008, 3, 444.
22. Tsai, J. L.; Tzeng S. H.; Chiu, Y. T. Compos B Eng 2010, 41, 106.
23. Chen, D.; Liu, T.; Zhou, X.; Tjiu, W. C.; Hou, H. J Phys Chem B 2009, 113, 9741.
24. Wu, K. L.; Chou, S. C.; Cheng, Y.Y. J Appl Polym Sci 2010, 116, 3111.
25. Zhu, B. K.; Xie, S. H.; Xu, Z. K.; Xu, Y.Y. Compos Sci Technol 2006, 66, 548.
26. He, G.; Zhou, J.; Tan, K.; Li, H. Comp Sci Technol 2011, 71, 1914.
27. Zhang, Z. L.; Li, B.; Shi, Z. J.; Gu, Z. N.; Xue, Z. Q.; Peng, L. M. J Mater Res 2000, 15, 2658.
28. Matsui, K.; Pradhan, B. K.; Kyotani, T.; Tamita, A. J Phys Chem B 2001, 105, 5682.